Spatio-temporal attributes of left ventricular pressure decay rate during isovolumic relaxation

Erina Ghosh[2] and Sándor J. Kovács[1,2]

[1]*Cardiovascular Biophysics Laboratory, Cardiovascular Division, Department of Internal Medicine, School of Medicine; and [2]Department of Biomedical Engineering, School of Engineering and Applied Science, Washington University, St. Louis, Missouri*

Ghosh E, Kovács SJ. Spatio-temporal attributes of left ventricular pressure decay rate during isovolumic relaxation. *Am J Physiol Heart Circ Physiol* 302: H1094–H1101, 2012. First published December 30, 2011; doi:10.1152/ajpheart.00990.2011.—Global left ventricular (LV) isovolumic relaxation rate has been characterized: *1*) via the time constant of isovolumic relaxation τ or *2*) via the logistic time constant τ_L. An alternate kinematic method, characterizes isovolumic relaxation (IVR) in accordance with Newton's Second Law. The model's parameters, stiffness E_k, and damping/relaxation μ result from best fit of model-predicted pressure to in vivo data. All three models (exponential, logistic, and kinematic) characterize global relaxation in terms of pressure decay rates. However, IVR is inhomogeneous and anisotropic. Apical and basal LV wall segments untwist at different times and rates, and transmural strain and strain rates differ due to the helically variable pitch of myocytes and sheets. Accordingly, we hypothesized that the exponential model (τ) or kinematic model (μ and E_k) parameters will elucidate the spatiotemporal variation of IVR rate. Left ventricular pressures in 20 subjects were recorded using a high-fidelity, multipressure transducer (3 cm apart) catheter. Simultaneous, dual-channel pressure data was plotted in the pressure phase-plane (dP/d*t* vs. P) and τ, μ, and E_k were computed in 1631 beats (average: 82 beats per subject). Tau differed significantly between the two channels ($P < 0.05$) in 16 of 20 subjects, whereas μ and E_k differed significantly ($P < 0.05$) in all 20 subjects. These results show that quantifying the relaxation rate from data recorded at a single location has limitations. Moreover, kinematic model based analysis allows characterization of restoring (recoil) forces and resistive (crossbridge uncoupling) forces during IVR and their spatio-temporal dependence, thereby elucidating the relative roles of stiffness vs. relaxation as IVR rate determinants.

diastolic function; catheterization; hemodynamics

ABNORMAL LEFT VENTRICULAR (LV) chamber relaxation is a known major determinant of diastolic dysfunction (22). Relaxation begins during late ejection and continues through early rapid filling and ends by diastasis, when the equilibrium (fully relaxed) volume is achieved (25). Isovolumic relaxation (IVR) duration (60–90 ms) is from aortic valve closure to mitral valve opening. IVR is only slightly heart rate dependent. In addition to using the IVR time interval as an index of relaxation, segments of the IVR pressure contour have been used. The isovolumic pressure contour from just beyond peak −dP/d*t* to just before mitral valve opening has been fit using a monoexponential by Weiss et al (29). The assumed exponential pressure decay rate relation is fit to recorded pressure using three parameters: τ, the time constant of IVR, P_o, the LV

pressure (in mmHg) at peak −dP/d*t*, and P_∞, the asymptote to which pressure declines. The pressure decay relation is:

$$P(t) = P_\infty + P_o e^{(-t/\tau)} \tag{1}$$

where τ is the e-folding time, the time it takes for the pressure to drop by a factor of 1/e. It is used clinically to assess relaxation rate as a diastolic function index (28). Prolongation of τ relative to normal is associated with the "delayed relaxation" pattern observed in Doppler echocardiographic transmitral Doppler E waves.

Matsubara's (18) isovolumic pressure decay model employs a logistic relationship where the isovolumic pressure decay relation beyond peak −dP/d*t* is:

$$P(t) = \frac{P_A}{[1 + \exp(-t/\tau_L)]} + P_B \tag{2}$$

where P_A is amplitude constant, P_B is pressure asymptote, and τ_L is the logistic time constant.

A third isovolumic pressure decay model uses Newton's Second Law in accordance with the (slight) known motion of tissue (chamber shape change) during IVR (5). It is a kinematic model that predicts IVR pressure from before peak −dP/d*t* to near mitral valve opening. Pressure decay is due to cross bridge uncoupling unmasking stored elastic [titin (17), extracellular matrix (23), and visceral pericardium (15) etc.] recoil/restoring forces that oppose the decaying contractile forces. The model is parametrized by stiffness (restoring) E_k and damping/relaxation μ. The differential equation for LV pressure during this phase of IVR is:

$$\frac{d^2 P}{dt^2} + \frac{1}{\mu}\frac{dP}{dt} + E_k(P - P_\infty) = 0 \tag{3}$$

where P_∞ represents the pressure asymptote. These parameters can be uniquely determined from each IVR pressure contour by solving the "inverse problem," i.e., by using appropriate mathematical methods to fit the model predicted solution to the experimentally recorded pressure and dP/d*t* data.

All these methods have been used to quantify global LV relaxation rates. However, relaxation is spatially inhomogeneous as evidenced by different rates and amounts of untwisting during IVR (16). The LV wall is constructed of helically woven layers and sheets of myocardial fibers (including extracellular matrix) assembled in interwoven sheets (4) such that fiber orientation changes both transmurally and along the long axis of the ventricle. This geometric arrangement generates the spatially and temporally inhomogeneous relaxation pattern accounting for observed intraventricular pressure gradients during filling. The intraventricular pressure gradients have

been studied previously by various groups using both noninvasive methods such as echocardiography (2) and MRI (10) and invasive methods such as catheterization (27). Most of these studies have focused on calculating atrioventricular or intraventricular pressure gradients during filling, rather than during IVR, when all valves are closed. Typically, any pressure differences within the LV at the instant of mitral valve opening were not considered, thereby disregarding pre-mitral valve opening chamber relaxation rate phenomena.

However, in light of the known spatiotemporal dispersion of wall motion (twist and global shape change) during IVR as documented by ventriculography, tagged cardiac MRI (13), speckle tracking (1), strain, and strain-rate imaging, the expectation that different pressure decay rates develop at different spatial locations in the LV is justified. To validate this hypothesis, we recorded LV pressure using a multipressure transducer (3-cm spacing) catheter in the LV to determine if pressure decay rates differed at the two locations. Furthermore, we hypothesized that timing and magnitude of relaxation mechanisms would differ at the two transducer locations. For validation, we calculated τ (exponential model) and μ and E_k (kinematic model) from simultaneous LV pressure data from each transducer and performed a comparison. We interpreted our results in kinematic terms to elucidate physiologic mechanisms operative during IVR.

METHODS

Inclusion criteria and data collection. We analyzed data from 20 subjects selected from our Cardiovascular Biophysics Laboratory database of high-fidelity micromanometric triple pressure transducer recordings. Before data acquisition, subjects provided signed, informed consent for participation. These procedures were approved by the Institutional Review Board (Human Research Protection Office) at Washington University School of Medicine. The criteria for inclusion included normal sinus rhythm, absence of valvular abnormalities, and absence of wall motion abnormalities or bundle branch block on the ECG. Subject demographics are summarized in Table 1. All patients underwent elective cardiac catheterization at the request of a referring cardiologist. The data acquisition methods have been described previously (26). Briefly, high-fidelity simultaneous LV pressure-volume and aortic root pressure measurements were obtained using a 6-F triple transducer-tipped pigtail pressure-volume conductance catheter (SSD-1034; Millar Instruments, Houston, TX) amplified and calibrated via standard transducer control units (TC-510; Millar Instruments). The distal (apical) and middle (mid-LV) pressure transducers were located 3 cm apart. To minimize the potential influence that catheter placement may have on our data, we took care to achieve consistency and accuracy of catheter placement, within the realities and constraints imposed by clinical, in vivo methodology. This was achieved in every subject by *1)* using fluoroscopy to cross the aortic valve with the catheter, noting that both (distal and mid) pressure channels displayed LV pressure waveforms while the proximal (3rd) sensor displayed aortic root pressures. This guaranteed that both distal and mid-pressure transducers were indeed within the LV. *2)* The geometric spatial relation of the ascending aorta relative to the LV outflow track and chamber naturally guides all catheters along the long axis of the chamber. If ectopy was generated by the pigtail portion of the catheter stimulating the endocardium, rotation of the catheter to orient the plane of the pigtail away from the point of contact was done. This is a standard maneuver in diagnostic angiography when left ventriculography is performed using any pigtail catheter. *3)* Once stable baseline rhythm was documented, echocardiography was undertaken for simultaneous echohemodynamic data acquisition. Pressure signals were inputted to clinical monitoring systems (Quinton Diagnostics, Bothell, WA, or GE Healthcare, Milwaukee, WI) and a custom personal computer via a research interface (Sigma-5DF; CD Leycom, Zoetermeer, The Netherlands) at a sampling rate of 250 Hz. Conductance signals were also stored on the research interface but were not used in this study. The ejection fraction was computed from the suitably calibrated ventriculogram.

Hemodynamic data analysis. Pressure was converted for analysis via a custom Matlab script (Matlab 6.0; MathWorks, Natick, MA). Data sets were smoothed digitally by using a five-point average to suppress noise in the derivative (26), attenuating 50% of signal at 40 Hz and 90% above 60 Hz, followed by calculation of continuous dP/dt vs. time t from the smoothed data. For each beat, LV end-diastolic pressure (LVEDP) and peak negative dP/dt denoted $(dP/dt)_{min}$ were extracted from the pressure phase-plane (dP/dt vs. P; PPP) or equivalent time-domain contours for both pressure signals.

Table 1. *Subject demographics: age, weight, LV end-diastolic pressure, ejection fraction, mean heart rate, and number of beats analyzed per subject*

Subject No.	Age, yr	Weight, lb	EDP, mmHg	Ejection Fraction, %	Heart Rate, beats/min	No. of Beats Analyzed
1	46	180	21	74%	61	99
2	66	200	14	60%	60	85
3	45	240	16	67%	75	36
4	53	135	14	74%	72	66
5	51	172	14	77%	52	74
6	52	194	11	72%	73	80
7	57	154	16	62%	76	63
8	58	115	13	85%	90	104
9	70	180	16	79%	92	85
10	75	175	12	73%	59	90
11	74	196	15	75%	59	89
12	54	161	13	63%	65	94
13	49	155	16	64%	56	83
14	55	165	17	54%	60	63
15	**79**	**159**	**15**	**48%**	**60**	**90**
16	61	175	15	75%	57	99
17	43	335	16	81%	59	85
18	57	290	20	86%	54	85
19	66	135	22	80%	55	77
20	69	178	15	62%	76	84

See text for details. EDP, end-diastolic pressure; LV, left ventricular. Boldface indicates subject with ejection fraction <50%.

Exponential model fits. A custom Matlab script performed the exponential (*Eq. 1*) fit to the pressure contours. Apical and mid-LV pressures were plotted in the PPP (12) (as shown in Fig. 1, *C* and *D*). According to convention (5) the segment starting from 4 ms after $(dP/dt)_{min}$ to 4 ms before mitral valve opening was used to determine τ. The IVR segment of the PPP is well approximated by a straight line as shown in Fig. 2*A*, with slope $-1/\tau$. This method was used to calculate τ for both mid-LV and apical pressure contours. Asymptotic pressure, P_∞, was calculated from the intercept of this line along the pressure axis.

Kinematic model fits. Kinematic model parameters (μ and E_k) were determined as previously (5, 26) using the Levenberg-Marquardt algorithm. The start point for fitting was defined by a drop in $d^2P(t)/dt^2$ of one-half after the inflection point in dP/dt, which defined $\dot{P}_o$. Data were fit until 5 ms before mitral valve opening pressure (defined by LVEDP). The algorithm provided parameters for μ, E_k, P_o, and P_∞ were calculated by minimizing the root mean squared error in fitting $P(t)$. This was implemented using Matlab, and the model parameters were calculated for each cardiac cycle. (Fig. 2, *B* and *C*).

Statistical analysis. The unsurpassed sensitivity of micromanometric (piezoelectric) pressure recording also includes noise. Hence, to eliminate noisy beats, we calculated the correlation between the actual data and the model derived (exponential and kinematic) fits using Pearson's correlation coefficient for each beat. Beats, in which the correlation coefficient (R^2) was <0.97 for either pressure channel, were excluded from analysis. After this filtering, 1,631 beats were selected. The exponential and kinematic model parameters were calculated as previously for both pressure channels. The two-tailed Student's *t*-test was used to compare apical and mid-LV relaxation parameters in each subject. A value of $P <$ 0.05 was considered significant.

Additionally, to evaluate how well each parameter, τ, P_∞, μ, and E_k, could differentiate between the two locations, a percent difference was calculated for each parameter. This percent difference was calculated by dividing the difference in the values by the average of the parameter values at the two locations.

RESULTS

We selected 20 data sets (mean age 59 yr) that comprised a typical cross section of our database (mean age: 58.6 yr) and analyzed 1,631 beats from these 20 patients ($\sim 82 \pm 16$ beats per person, 13 men). Patient demographics are shown in Table
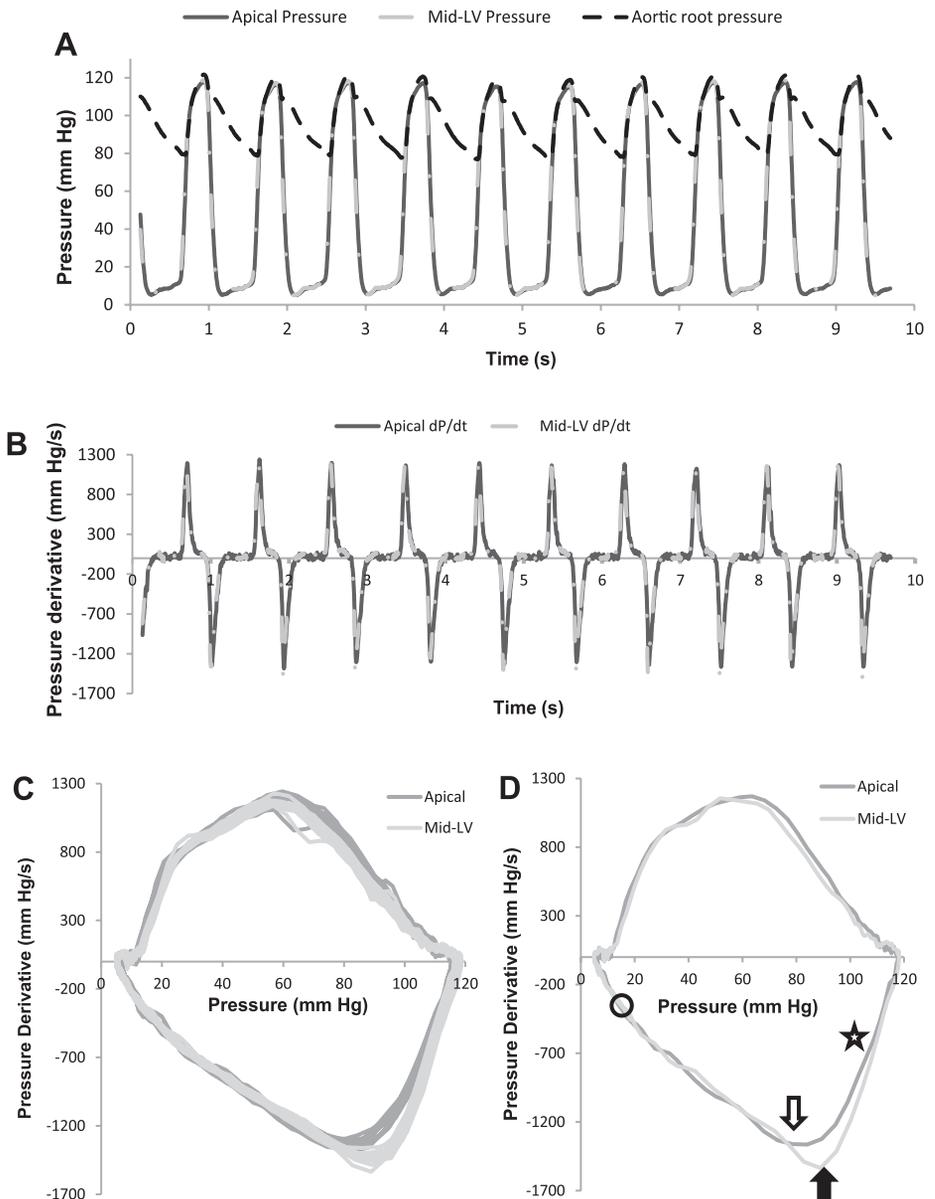

Fig. 1. Typical pressure data from 1 subject. Solid line, 1st transducer (LV apex); grey dashed line, 2nd transducer [mid left ventricular (LV)]; black dashed line, 3rd transducer (aortic root pressure). *A*: pressure as a function of time, all 3 transducers, 10 consecutive beats. *B*: pressure derivative (dP/dt) as a function of time for data in *A*. *C*: pressure phase-plane (dP/dt vs. P), for data in *A* only the apical and mid-left ventricular (LV) pressures are shown. *D*: for clarity single cardiac cycle shown inscribes a clockwise loop. Star denotes isovolumic relaxation (IVR) onset, solid up arrow is mid-LV dP/dt$_{min}$, down arrow is apical dP/dt$_{min}$, and circle is IVR termination. See text for details.
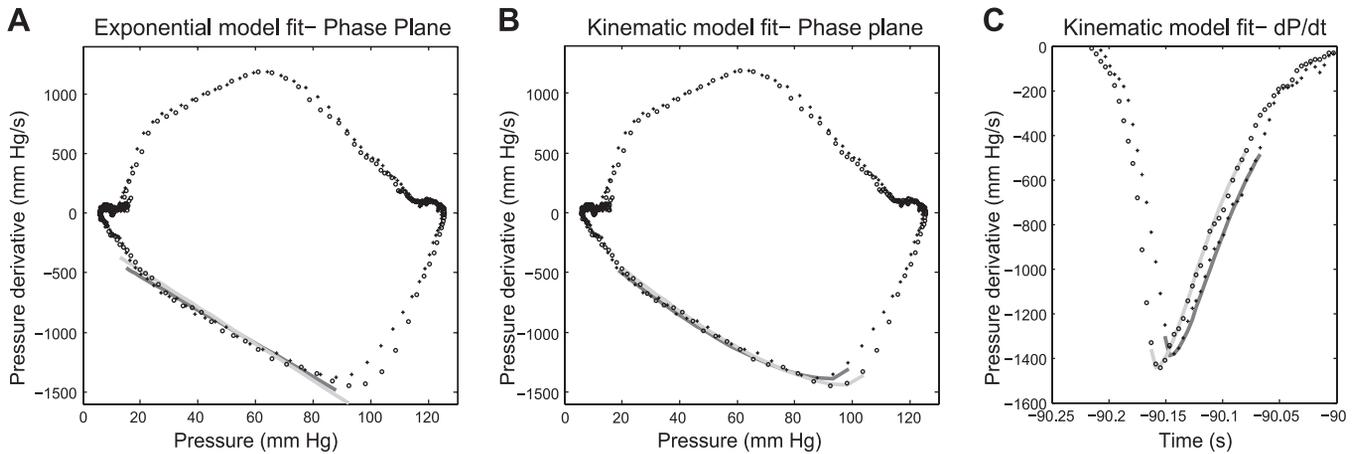
Fig. 2. Pressure phase-plane comparison of tau model and kinematic model fits for 1 cardiac cycle. Same subject as Fig.1. LV apex pressure (+) and mid-LV pressure (o). *A*: τ-model fit τ_{apex} = 71 ms and τ_{mid} =65 ms. Apical pressure fit (dark grey) and mid-LV pressure fit (light grey) are shown. Note τ-model fit utilizes data only after peak negative dP/dt. *B*: kinematic fit to same data. The μ_{apex} = 1.6 ms, $E_{k,apex}$ = 872.42 s^{-2}, μ_{Mid} = 1.57 ms, and $E_{k,Mid}$ = 916 s^{-2}. Apical pressure fit (dark grey) and mid-LV pressure fit (light grey) are shown. *C*: kinematic model predicted fit to dP/dt vs. time data. Note kinematic fit includes data before and after peak negative dP/dt. See text for details.

1. To assure physiologic robustness, we took care to include a representative range diastolic function, from low normal to elevated LVEDP, commonly encountered in such a group. Nineteen of the 20 subjects had a normal ejection fraction (EF > 50%). The mean EF of the group was $71 \pm 10\%$. The mean LVEDP varied from 11 to 22 mmHg (16 ± 3 mmHg). In the study, nine subjects had LVEDP < 15 mmHg, nine subjects had LVEDP between 15 and 20 mmHg, and two subjects had LVEDP > 20 mmHg. The heart rate for the group was 66 ± 12 beats/min. Table 1 lists weight, LVEDP, ejection fraction, mean heart rate, and the number of beats analyzed for each subject. Thirteen of 20 subjects had a distinct diastatic interval on transmitral echo.

Figure 1 shows typical data for both PPP and P vs. *t* plots. Figure 1*A* shows 10 beats from a selected subject. Apical (solid black) and mid-LV (dashed grey) pressures are shown. Dashed black is aortic root pressure from the third, most-proximal

transducer. Figure 1*B* shows the pressure derivative (dP/dt) for the same beats as a function of time. Figure 1*C* shows the PPP plot for the 10 beats (all 3 transducers). Figure 1*D* shows one cardiac cycle in the PPP (all 3 transducers) for clarity. Figure 2, *A* and *B*, compares the exponential fit and the kinematic model fit to the same beat. Figure 2*C* shows the same data as Fig. 2*B* on a dP/dt vs. *t* plot.

Due to the availability of a large number of beats for analysis, subject comparisons utilized mean values for the parameters for each subject. Table 2 lists τ (means ± SD) for the two recording sites, τ_{mid} and τ_{apex}. The fourth column lists the *P* value per subject. With the use of $P < 0.05$ to indicate statistical significance, 16 of the 20 subjects had significantly different values of τ between the two transducers. In 17 of the 20 subjects, τ_{apex} was greater than τ_{mid}. The subjects in whom τ_{apex} was less than τ_{mid}, the difference was not statistically significant. Asymptotic pressures were also calculated (Table

Table 2. *Mean τ, P∞ (apex, mid), and P values*

Subject No.	τ_{apex}, ms	τ_{Mid}, ms	*P* Value	$P_{\infty,apex}$, mmHg	$P_{\infty,Mid}$, mmHg	*P* Value
1	63 ± 4	61 ± 3	<0.0001	−4.3 ± 3.2	−3.7 ± 2.3	0.008
2	56 ± 2	54 ± 2	<0.0001	−6.1 ± 2.8	−4.4 ± 2.5	<0.0001
3	73 ± 6	68 ± 5	<0.0001	−9.9 ± 6.5	−6.2 ± 6.5	<0.0001
4	54 ± 5	52 ± 4	<0.0001	−9.5 ± 4.3	−7 ± 3.2	<0.0001
5	67 ± 4	62 ± 8	<0.0001	−15.8 ± 4.4	−8.2 ± 5.8	<0.0001
6	65 ± 5	62 ± 3	<0.0001	−14.8 ± 5.1	−8.9 ± 3.6	<0.0001
7	65 ± 5	62 ± 4	<0.0001	−11.1 ± 7	−10.3 ± 6	0.03
8	45 ± 8	44 ± 8	0.02	−7 ± 3.8	−6.5 ± 4.9	0.31*
9	55 ± 3	53 ± 3	<0.0001	−6.4 ± 3.6	−3.9 ± 3	<0.0001
10	62 ± 3	61 ± 2	0.008	−9.5 ± 3	−6.3 ± 2.2	<0.0001
11	73 ± 8	66 ± 6	<0.0001	−18.5 ± 8.4	−10.9 ± 6	<0.0001
12	66 ± 4	64 ± 3	<0.0001	−13.2 ± 2.9	−10.8 ± 2.1	<0.0001
13	**76 ± 5**	**75 ± 5**	**0.05***	**−17.7 ± 3.7**	**−13.7 ± 3.1**	**<0.0001**
14	**89 ± 11**	**89 ± 8**	**0.95***	**−22.8 ± 9.3**	**−20.5 ± 6.4**	**0.001**
15	71 ± 7	70 ± 6	0.0002	−13.1 ± 7.4	−11.5 ± 6.6	<0.0001
16	60 ± 4	58 ± 5	0.004	−5.2 ± 4.1	−4.7 ± 4.2	0.02
17	69 ± 6	66 ± 5	<0.0001	−3.6 ± 3.4	−1.3 ± 3.1	<0.0001
18	82 ± 4	79 ± 3	<0.0001	−12.6 ± 5.5	−11.1 ± 4.6	<0.0001
19	**66 ± 9**	**66 ± 7**	**0.42***	**−19.6 ± 8.9**	**−14.3 ± 6.8**	**<0.0001**
20	**64 ± 4**	**64 ± 4**	**0.25***	**−14.9 ± 6.2**	**−13.6 ± 5.2**	**<0.0001**

Values are means ± SE. τ, Time constant of isovolumic relaxation at apical (apex) and mid-LV (mid). P∞, pressure asymptote. $P < 0.05$ denotes significant. *$P > 0.05$ values. These subjects are also highlighted in bold. See text for details.

2). The asymptotic pressure fitting parameter P_∞ was statistically different at the 2 locations in 19 subjects and the apical P_∞ was greater in magnitude than mid-LV P_∞ in all subjects.

The data were also fit using the kinematic model to determine μ and E_k. Table 3 shows μ and E_k values (means $\pm$ SD) for the apical and mid-LV pressure transducers. The fourth and seventh columns indicate the P values for μ and E_k respectively. Using $P < 0.05$ for statistical significance, we found that all 20 subjects had μ and E_k values, which were statistically significantly different between the two spatial locations. The subjects in which the τ_{mid} and τ_{apex} were not statistically significantly different are denoted in bold.

The percentage difference between mid-LV and apical transducer τ-values ranged from 0.1 to 10.6% (mean: 3.5%). The percentage difference between mid-LV and apical transducer μ-values ranged from 5.3 to 95.5% (mean: 33%). The percentage difference between mid-LV and apical transducer E_k ranged from 2.2 to 78.9% (mean: 46%).

Of the 20 subjects 13 had clearly discernible diastatic interval (separated Doppler E and A waves). Five had Doppler E waves with A-wave onset at E-wave termination, hence, no diastatic interval. The remaining two had A waves that merged with the end of the Doppler E wave. To determine if the presence or absence of diastasis influenced the results, we compared the average mid-LV and apical τ, P_∞, μ, and E_k values in subjects with and without diastasis. With the use of $P < 0.05$ criteria, μ, E_k, τ, and P_∞ for both locations were not statistically different.

DISCUSSION

It is established that the atrioventricular pressure gradient that generates the Doppler E wave also includes the observed intraventricular pressure gradients within the LV during the E wave itself. However, the spatio-temporal characteristics of LVP during isovolumic relaxation, before mitral valve opening are unknown. In light of the known spatiotemporal heterogeneity of wall motion during IVR, we hypothesized that relaxation rate heterogeneity can be quantified by spatial differences in pressure decay rate during IVR. For validation, simultaneously recorded isovolumic pressure data from two locations in the LV (apex and mid-LV, 3 cm apart) were fit using both the exponential (Weiss) and kinematic (Chung) pressure decay models. Both models generated statistically different relaxation rate parameters (between locations), thereby characterizing spatially different isovolumic relaxation rates. We also sought to understand the physiology responsible for differential relaxation rates.

Previous studies. Pressure gradients during filling have been previously reported using invasive and noninvasive methods (2, 8, 24). Courtois et al. (7, 8) measured the Doppler E-wave features and intraventricular regional pressure variation during the E wave in a canine, closed chest model. Nikolic et al. (19) measured intraventricular pressure gradients in early diastole for both filling and nonfilling beats in dogs. They related the pressure gradients to elastic recoil and ventricular shape changes. In addition, intraventricular pressure gradients of 3 mmHg during early filling (Doppler E wave) have also been observed via color M-mode echocardiography (19, 27).

All these studies focus on pressure gradients after mitral valve opening. Intraventricular pressure gradients during the IVR phase have not been considered. Sasson et al. (24) recorded intraventricular, apically directed flow during IVR using continuous wave Doppler echocardiography, but relaxation rates were not considered in the study. Pioneering work regarding IVR has been performed by Davis et al. (9) where the variation of τ from base to apex in an open chest canine model involving transapical and transatrial puncture, was studied using a single transducer catheter. Pressure was measured by moving the catheter to six different locations in the canine LV. Three different methods of analysis were used to calculate τ. They found conflicting results in the trend of spatial variation of τ depending on the method of analysis. In concordance with our observations, they reported that τ increased from the base to apex using *Eq. 1*. However, using an error minimizing

Table 3. *Kinematic model parameters*

Subject No.	Apical μ, ms	Mid-LV μ, ms	P Value	Apical E_k, $1/s^2$	Mid-LV E_k, $1/s^2$	P Value
1	11 ± 3	6 ± 2	<0.0001	1,619 ± 591	2,646 ± 841	<0.0001
2	10 ± 3	6 ± 2	<0.0001	1,804 ± 513	3,235 ± 954	<0.0001
3	13 ± 4	8 ± 2	<0.0001	1,317 ± 445	2,095 ± 605	<0.0001
4	14 ± 2	12 ± 2	<0.0001	1,319 ± 230	1,446 ± 261	<0.0001
5	9 ± 2	7 ± 2	<0.0001	1,639 ± 411	3,019 ± 1733	<0.0001
6	16 ± 5	11 ± 2	<0.0001	1,126 ± 306	1,577 ± 377	<0.0001
7	15 ± 2	14 ± 5	0.004	1,078 ± 280	1,310 ± 990	<0.0001
8	11 ± 2	7 ± 3	<0.0001	2,017 ± 350	3,818 ± 1530	<0.0001
9	13 ± 3	9 ± 2	<0.0001	1,402 ± 222	1,955 ± 399	<0.0001
10	10 ± 4	6 ± 2	<0.0001	1,705 ± 684	2,884 ± 937	<0.0001
11	12 ± 3	8 ± 3	<0.0001	1,233 ± 343	1,962 ± 621	<0.0001
12	11 ± 3	8 ± 2	<0.0001	1,368 ± 315	1,888 ± 541	<0.0001
13	**15 ± 3**	**9 ± 5**	**<0.0001**	**991 ± 213**	**2,169 ± 1459**	**<0.0001**
14	**17 ± 3**	**15 ± 4**	**<0.0001**	**751 ± 152**	**834 ± 280**	**0.0005**
15	13 ± 4	10 ± 4	<0.0001	1,210 ± 453	1,610 ± 997	<0.0001
16	14 ± 8	10 ± 3	<0.0001	1,434 ± 581	1,797 ± 647	<0.0001
17	12 ± 4	4 ± 2	<0.0001	1,338 ± 596	4,471 ± 2532	<0.0001
18	16 ± 4	12 ± 4	<0.0001	824 ± 241	1,056 ± 393	<0.0001
19	**14 ± 3**	**13 ± 3**	**<0.0001**	**1,148 ± 300**	**1,232 ± 343**	**<0.0001**
20	**17 ± 5**	**15 ± 3**	**<0.0001**	**984 ± 181**	**1,042 ± 217**	**<0.0001**

Values are means $\pm$ SE. Mean damping/relaxation (μ) and stiffness (E_k) values from apical and mid-LV pressure data including P values. For comparison, τ-values having $P > 0.05$ (from Table 2) are in bold. See text for details.

algorithm to estimate τ and P_∞ they arrived at the opposite conclusion. Their work showed that τ varied in the LV with changes in transducer location, limited by uncertainty regarding the pattern of variation and potential mechanistic explanations.

Difference in τ_{apex} vs. τ_{mid} from the exponential model. We used the monoexponential (Weiss) model to evaluate relaxation rate for simultaneously measured apical and mid-LV pressures. We found 16 of 20 subjects had statistically different values for τ_{apex} vs. τ_{mid} (Table 2). The τ_{apex} was greater than τ_{mid} in 17 of the 20 subjects. In four of the subjects, statistically significant difference between τ_{apex} vs. τ_{mid} was not observed. Some contributing factors for this include choice of method for calculating τ (9), fidelity of data acquisition, data processing techniques, etc. In addition, when two simultaneous pressures are measured, the hydrostatic position of the pressure sensors in the LV and the orientation of the LV itself and that of the catheter with respect to the LV may also play a role. The exact position of the pressure transducers in a given LV is somewhat variable (for example to avoid catheter induced ectopy), while the orientation of the catheter in general is along the long axis of the chamber, as verified by echocardiography during data acquisition, but in location with respect to the apex, some variability is unavoidable.

The calculated P_∞ values were negative. The apical P_∞ was significantly lower than the mid-LV P_∞. This implies that apical recoil generates a lower P_∞. It is consistent with achieving the lowest pressure in a completely relaxed ventricle (in case of no filling; Ref. 19).

Differences in kinematic model parameters. To elucidate and characterize mechanistic attributes of relaxation rate beyond Weiss' exponential model's capabilities, we used Chung's kinematic model (5), which commences before dP/dt_{min} until mitral valve opening. It provides a better fit for wider range of PPP contours (26; Fig. 2) than the τ model. We calculated the kinematic model parameters for the simultaneous, dual pressure data (Table 3). In contrast to τ, kinematic model parameters were statistically significantly different in every subject. We found $\mu_{apex} > \mu_{mid}$ in all subjects and $E_{k,mid} > E_{k,apex}$ in all subjects.

The numerical difference in μ and E_k values at the two locations is larger than the numerical difference in τ-values. Numerically, the difference in τ was $\approx 3\%$ of the actual value, whereas the difference in μ was 33% of the actual value and the difference in E_k was 46% of the actual value. Hence, the kinematic model is more sensitive to spatial heterogeneity in rate of pressure decay than the exponential (τ) model.

Pattern of intraventricular pressure decay. The difference in pressure and pressure derivative (dP/dt) between the apex and mid-LV is clearly displayed in the PPP plots (Fig. 1, *C* and *D*). Figure 1*D* shows that after the aortic valve closes (denoted by star) mid-LV pressure decreases faster [evidenced by the higher magnitude of dP/dt (mid-LV)] than apex. This continues until dP/dt_{min} is reached (solid arrow for mid-LV and open arrow for apex) and after these minima, dP/dt starts to increase for both. During this portion of IVR, the differences in dP/dt magnitude at the two locations are smaller than the differences before dP/dt_{min}. These differences in slopes cannot be appreciated in Fig. 1, *A* or *B*, due to the large range of values of pressure (10–120 mmHg) and dP/dt (−1,500 to 1,300

mmHg/s) relative to the difference in the values at the two locations.

The exponential model fits the PPP segment after dP/dt_{min} till near mitral valve opening (Fig. 1*D*, open circle). During this part of IVR, we found that τ_{apex} is greater than τ_{mid}. This implies that apical relaxation rate is slower than mid-LV relaxation rate, seen in Fig. 2*A* where the fit to the mid-LV (light grey) is steeper than the apical (dark grey) fit. Although the τ-model does not provide mechanistic insight regarding the rate of pressure decay during IVR, the data indicate that the relaxation rate depends on spatial location.

The kinematic model assumes that pressure decay is determined by the interplay of stored elastic restoring force overcoming the opposing, but decaying, contractile forces as a result of crossbridge uncoupling. After aortic valve closure, stored elastic restoring forces dominate the decaying contractile forces thereby accelerating the rate of pressure decay magnitude until the peak rate of pressure decay, dP/dt_{min}, is reached. At the instant of dP/dt_{min}, the restoring force and the damping force are precisely balanced, and the second derivative of pressure, d^{2}P/dt^2, is zero. After this point, damping (resistive) force dominates restoring force and slows the rate of relaxation.

Our model-based fit to the data reveal that stiffness, E_k, is higher in the mid-LV than the apex. Thus the kinematic restoring force is higher in the mid-LV, encountered during the initial part of IVR (i.e., before mid-LV dP/dt_{min}), and the rate of pressure decay (dP/dt) is faster in mid-LV than the apex (Fig. 1*D*). This is also corroborated by the dP/dt vs. time plot (Fig. 2*C*) where the decrease in dP/dt (mid-LV) is faster than dP/dt (apex). The mid-LV pressure contour reaches its minimum value first (Fig. 2*C*). After dP/dt_{min}, the balance of forces changes sign and damping forces dominate pressure decay (as seen by the decreasing magnitude of dP/dt). The μ_{apex} is higher than μ_{mid-LV}. Since the damping force is inversely proportional to μ, the mid-LV pressure decay is more damped. Hence, the apical dP/dt is less damped and decays (in magnitude) slower as shown in Figs. 1*D* and 2*C*. This agrees with the results of the exponential model, which also showed that apical relaxation proceeds at a slower rate.

The quantification of relaxation rate by the two models also proves that the pressure gradients are caused not only by a temporal difference in the onset of relaxation at different locations but also by inherent differences in chamber kinematic properties (stiffness and relaxation) at the different locations themselves. If intraventricular pressure gradients were solely caused by differences in the onset of relaxation at the mid-LV and apex, then there would not be any difference in chamber parameters (τ, μ, and E_k) and relaxation rates between the two locations, and the two dP/dt contours (Fig. 2*C*) could be superimposed by shifting the contour in time, which is not the case.

Intraventricular pressure differences during filling have been previously calculated from color Doppler M-mode data and velocity of propagation V_p (11). Because V_p is zero during IVR, a pressure gradient cannot be calculated. Hence, although a pressure difference has been noted during early filling, not much is known about the relaxation rates operative during IVR. Using two different models of pressure decay, we have shown that the parameters determining the rate of pressure decay are significantly different at two different locations. This extends the work of Davis

et al. (9) where they noted the variation in τ as a function of intraventricular location. Our results agree with their results in terms of similar trends of τ variation in the LV and a similar coefficient of correlation between the exponential fit and the actual data ($R^2 = 0.98$ in both the studies). Our study has the advantage of being performed in humans under closed chest, physiologic conditions, implying clinical translational potential. Furthermore, analyzing the data via the kinematic model of IVR has allowed us to elucidate and further characterize the physiology underlying the mechanism of intraventricular pressure decay rate variation. Recent studies (6) have shown that the PEVK region of titin generates resistive (i.e., viscous) forces by transiently interacting with actin during LV relaxation. Other studies (3, 15, 20) characterized the role of extracellular matrix in contributing to passive LV mechanical properties. Although these studies have not looked at IVR specifically, they demonstrate that stiffness and damping (viscosity relaxation) have cellular and subcellular analogs. Therefore, it is reasonable to interpret our results as evidence for the spatial dependence of stiffness and relaxation elements of the chamber.

Beyond facilitating interpretation of the physiology in kinematic terms, an advantage of the kinematic approach resides in its ability to fit the PPP contour from before dP/dt_{min} as shown in Fig. 2B. The initial conditions of the fit, dP/dt_o (rate of relaxation), before the minima affects the rate of relaxation after. The relative rates (apical vs. mid-LV) are influenced by dP/dt_{min} values, which is taken into account only by the kinematic model. Hence, kinematic modeling of IVR process facilitates mechanistic understanding of pressure decay attributes during IVR.

Significance and future work. In this study, we investigated the differences in rates of isovolumic pressure decay at different locations in the LV and sought to understand it in causal, physiologic, mechanistic terms. Our results show that the mechanics of relaxation differ depending on spatial location. This is important because it affects how we interpret the results of experiments using isovolumic relaxation rates (τ). Studies (14, 21) often use τ to quantify the relaxation rate of the LV and to differentiate between groups or the effect of an intervention. However, prior studies failed to consider the spatial variation in τ, which has a bearing on the significance of conclusions drawn based on variation in τ.

The method used in this study can quantify alterations in LV relaxation rates in selected pathological conditions. Moreover, given our current knowledge of how relaxation rate depends on spatial location, the future study of intraventricular pressure gradients during IVR and their relation to suction (dP/dV < 0) during the E wave should be particularly enlightening. Additionally, the magnitude of intraventricular pressure gradients could be used as potential predictor of early diastolic filling.

Limitations. The main limitations pertain to data acquisition methods. As noted previously (23), calibration, catheter placement, and orientation with respect to the LV axis may influence pressure recordings. However, calibration issues will affect both pressure channels equally and offsets the pressure by a constant value. This should not affect the model's pressure decay rate parameter (μ) since it is fit to dP/dt. Calibration and drift are mitigated by pre- and postcalibration of transducers to zero hydrostatic pressure in a 37°C saline bath. Precise orientation within the LV from subject to subject is not possible beyond orientation along the long-axis of the chamber after

crossing the aortic valve and positioning to exclude catheter induced ectopy. The consistency of apical and mid-LV locations is assured by echocardiographic imaging of the catheter in the LV using the parasternal long axis view. Hence, within practical anatomic constraints, our data represent measurement of the apical and mid-LV region.

Other issues may involve signal processing, which we have addressed previously (26). Another limitation concerns subjects in whom the diastatic interval was zero. Since diastasis defines the in vivo equilibrium volume of the LV (25), when a diastatic interval is not clearly present the LV may not have completely relaxed before atrial filling onset. This might influence our conclusions and the parameters computed from the data for the previous IVR interval. To check this, we compared the model parameters: τ, P_∞, μ, and E_k among the subjects with and without clear diastasis and found no statistical difference between the two groups (see RESULTS).

In this physiologic study, we selected data sets of 20 subjects with essentially normal EFs (19 subjects EF > 50%) and a wide range of LVEDP (range: 11 to 22 mmHg) characteristic of what one encounters in clinical practice. Our goal was to quantify physiology in terms of the spatial differences in relaxation rates within the LV. The performance of a clinical study, which compares normal vs. pathologic cases with respect to changes in rate of pressure decay (and model parameters) as a function of location within the LV in different pathologic subsets, is reserved for future work.

Conclusion. The time constant of isovolumic relaxation τ and the kinematic model of isovolumic pressure decay were employed to elucidate and characterize spatiotemporal physiologic IVR mechanisms. Our results demonstrate that isovolumic relaxation rates at 2 locations in the LV, 3 cm apart, are distinguishable. Although τ is conventionally used to measure the global relaxation component of diastolic function (30), its ability to provide the full picture is limited. In contrast, kinematic model-based analysis of IVR allows characterization of whether and when during IVR restoring (recoil) forces dominate resistive (crossbridge uncoupling) forces and their spatiotemporal dependence. Because relaxation proceeds at different rates in different regions of the LV, reliance on data recorded at a single location in the LV has limitations. The physiological significance of these findings are as follows: *1*) all hearts decrease their pressures during IVR by the same physiologic mechanism of stored elastic strain generated recoil modulated by crossbridge uncoupling, *2*) these processes can be quantified via *Eq. 3* (Chung equation) by direct determination of stiffness (E_k) and relaxation (viscosity μ) from in vivo data, and *3*) the relative values of E_k and μ at different spatial locations determine the dominance of each of these forces including their potential dependence on pathology. Application in specific clinical subsets including assessment of model parameter variation in response to selected pharmacologic agents intended to treat diastolic dysfunction is warranted.

DISCLOSURES

No conflicts of interest, financial or otherwise, are declared by the author(s).

AUTHOR CONTRIBUTIONS

Author contributions: E.G. and S.J.K. conception and design of research; E.G. analyzed data; E.G. and S.J.K. interpreted results of experiments; E.G. prepared figures; E.G. and S.J.K. drafted manuscript; E.G. and S.J.K. edited and revised manuscript; E.G. and S.J.K. approved final version of manuscript; S.J.K. performed experiments.

REFERENCES

1. **Al-Naami GH.** Torsion of young hearts: a speckle tracking study of normal infants, children and adolescents. *Eur J Echocardiogr* 11: 853–862, 2010.
2. **Bermejo J, Antoranz JC, Yotti R, Moreno M, García-Fernández MA.** Spatio-temporal mapping of intracardiac pressure gradients. A solution to Euler's equation from digital postprocessing of color Doppler M-mode echocardiograms. *Ultrasound Med Biol* 27: 621–630, 2001.
3. **Brower GL, Gardner JD, Forman MF, Murray DB, Voloshenyuk T, Levick SP, Janicki JS.** The relationship between myocardial extracellular matrix remodeling and ventricular function. *Eur J Cardiothorac Surg* 30: 604–610, 2006.
4. **Buckberg G, Mahajan A, Saleh S, Hoffman JIE, Coghlan C.** Structure and function relationship of the helical ventricular myocardial band. *J Thorac Cardiovasc Surg* 136: 578–589, 2008.
5. **Chung CS, Kovács SJ.** Physical determinants of left ventricular isovolumic pressure decline: model prediction with in vivo validation. *Am J Physiol Heart Circ Physiol* 294: H1589–H1596, 2008.
6. **Chung CS, Methawasin M, Nelson OL, Radke MH, Hidalgo CG, Gotthardt M, Granzier HL.** Titin based viscosity in ventricular physiology: an integrative investigation of PEVK- actin interactions. *J Mol Cell Cardiol* 51: 428–434, 2011.
7. **Courtois MR, Kovács SJ Jr, Ludbrook PA.** Loss of early diastolic intraventricular pressure gradient during acute myocardial ischemia. *J Am Coll Cardiol* 13: 1218, 1989.
8. **Courtois MR, Kovács SJ Jr, Ludbrook PA.** Transmitral pressure-flow velocity relation. Importance of regional pressure gradients in the left ventricle during diastole. *Circulation* 78: 661–671, 1988.
9. **Davis KL, Mehlhorn U, Schertel ER, Geissler HJ, Trevas D, Laine GA, Allen SJ.** Variation in Tau, the time constant for isovolumic relaxation, along the left ventricular base-to-apex axis. *Basic Res Cardiol* 94: 41–48, 1999.
10. **Dong S, Hees PS, Siu CO, Weiss JL, Shapiro EP.** MRI assessment of LV relaxation by untwisting rate: a new isovolumic phase measure of τ. *Am J Physiol Heart Circ Physiol* 281: H2002–H2009, 2001.
11. **Ebbers T, Wigström L, Bolger AF, Wranne B, Karlsson M.** Noninvasive measurement of time-varying three-dimensional relative pressure fields within the human heart. *J Biomech Eng* 124: 288–293, 2002.
12. **Eucker SA, Lisauskas JB, Singh J, Kovács SJ Jr.** Phase-plane analysis of left ventricular hemodynamics. *J Appl Physiol* 90: 2238–2244, 2001.
13. **Götte MJW, Germans T, Rüssel IK, Zwanenburg JJM, Marcus JT, van Rossum AC, van Veldhuisen DJ.** Myocardial strain and torsion quantified by cardiovascular magnetic resonance tissue tagging: Studies in normal and impaired left ventricular function. *J Am Coll Cardiol* 48: 2002–2011, 2006.
14. **Ishida Y, Meisner JS, Tsujioka K, Gallo JI, Yoran C, Frater RW, Yellin EL.** Left ventricular filling dynamics: influence of left ventricular relaxation and left atrial pressure. *Circulation* 74: 187–196, 1986.
15. **Jöbsis PD, Ashikaga H, Wen H, Rothstein EC, Horvath KA, McVeigh ER, Balaban RS.** The visceral pericardium: macromolecular structure and contribution to passive mechanical properties of the left ventricle. *Am J Physiol Heart Circ Physiol* 293: H3379–H3387, 2007.
16. **Kerckhoffs RCP, Omens JH, McCulloch AD, Mulligan LJ.** Ventricular dilation and electrical dyssynchrony synergistically increase regional mechanical nonuniformity but not mechanical dyssynchrony. *Circ Heart Fail* 3: 528–536, 2010.
17. **LeWinter MM, Granzier H.** Cardiac titin. *Circulation* 121: 2137–2145, 2010.
18. **Matsubara H, Takaki M, Yasuhara S, Araki J, Suga H.** Logistic time constant isovolumic relaxation pressure- time curve in the canine left ventricle. *Circulation* 92: 2318–2326, 1995.
19. **Nikolic SD, Feneley MP, Pajaro OE, Rankin JS, Yellin EL.** Origin of regional pressure gradients in the left ventricle during early diastole. *Am J Physiol Heart Circ Physiol* 268: H550–H557, 1995.
20. **Nishimura S, Nagai S, Katoh M, Yamashita H, Saeki Y, Okada J, Hisada T, Nagai R, Sugiura S.** Microtubules modulate the stiffness of cardiomyocytes against shear stress. *Circ Res* 98: 81–87, 2006.
21. **Nitenberg A, Lecarpentier Y, Antony I, Chemla D.** Dipyridamole slows the rate of isovolumic pressure fall in patients with normal coronary arteries. *Eur Heart J* 16: 1721–1725, 1995.
22. **Ommen SR, Nishimura RA.** A clinical approach to the assessment of left ventricular diastolic function by Doppler echocardiography: update 2003. *Heart, Suppl* 89: iii8–iii23, 2003.
23. **Robinson TF, Factor SM, Sonnenblick EH.** The heart as a suction pump. *Sci Am* 254: 84–91, 1986.
24. **Sasson Z, Hatle L, Appleton CP, Jewett M, Alderman EL, Popp RL.** Intraventricular flow during isovolumic relaxation: description and characterization by Doppler echocardiography. *J Am Coll Cardiol* 10: 539-546, 1987.
25. **Shmuylovich L, Chung CS, Kovács SJ.** Last word on point: Counterpoint: Left ventricular volume during diastasis is the physiological in vivo equilibrium volume and is related to diastolic suction. *J Appl Physiol* 109: 612–614, 2010.
26. **Shmuylovich L, Kovács SJ.** Stiffness and relaxation components of the exponential and logistic time constants may be used to derive a load-independent index of isovolumic pressure decay. *Am J Physiol Heart Circ Physiol* 295: H2551–H2559, 2008.
27. **Steine K, Stugaard M, Smiseth OA.** Mechanisms of diastolic intraventrcular regional pressure differences and flow in the inflow and outflow tracts. *J Am Coll Cardiol* 40: 983–990, 2002.
28. **Stoddard MF, Pearson AC, Kern MJ, Ratcliff J, Mrosek DG, Labovitz AJ.** Left ventricular diastolic function: comparison of pulsed Doppler echocardiographic and hemodynamic indexes in subjects with and without coronary artery disease. *J Am Coll Cardiol* 13: 327–336, 1989.
29. **Weiss JL, Frederiksen JW, Weisfeldt ML.** Hemodynamics determinants of the time course of fall in canine left ventricular pressure. *J Clin Invest* 58: 751–760, 1976.
30. **Zile MR, Brutsaert DL.** New concepts in diastolic dysfunction and diastolic heart failure. Part I: diagnosis, prognosis, and measurements of diastolic function. *Circulation* 105: 1387–1393, 2002.